Modeling the motion of a toy car traveling on an arbitrarily shaped track

D. P. Wick[a)] and M. W. Ramsdell
Department of Physics, Clarkson University, Potsdam, New York 13699-5820

(Received 7 September 2001; accepted 5 April 2002)

An analysis is performed on the motion of a Matchbox car racing down an arbitrarily shaped track that resides in a two-dimensional vertical plane. The role of friction, track shape, and air resistance on the car's performance is investigated. The parameters that describe the car's effective coefficient of friction and drag constant are experimentally extracted by consideration of its motion on a flat, horizontal track. These parameters are then employed to make predictions of the velocity on an arbitrarily shaped track containing hills and valleys and compared with measured values. A rigidly mounted shield of varying cross-sectional area is used to enhance the effects of drag. This analysis has been successfully incorporated into an advanced group project for an introductory course in classical mechanics and can be customized to accommodate a variety of levels. © *2002 American Association of Physics Teachers.*
[DOI: 10.1119/1.1482061]

I. INTRODUCTION

Toy cars and air track carts are frequently used in introductory physics classes to demonstrate the exchange between gravitational potential and kinetic energy on an inclined plane. A simple experiment can be conducted to estimate frictional losses by using a single photogate or a motion detector to measure the velocity and acceleration of a car.[1,2] An effective friction coefficient can be obtained by comparing cases with the car moving up and down the plane. A similar approach can be employed to estimate the effects of air resistance.[3] Typically, both effects are not considered simultaneously.

We present a quantitative analysis of the motion of a toy car (Matchbox™) traveling on an arbitrarily shaped track residing in a two-dimensional vertical plane. Attention is given to the role of friction, track shape (curvature), and air resistance on the car's performance. The effective coefficient of friction and drag constant are experimentally extracted by consideration of the motion on a flat, horizontal track. An exact solution to the equation of motion for this case allows us to determine these parameters based on velocity measurements taken with a series of photogates. These parameters can then be used to make numerical predictions of the velocity for a car moving on an arbitrarily shaped track allowing for a frictional force that varies according to the curvature. Rigidly mounted shields of varying cross-sectional area are used to enhance the effects of air resistance. The numerical solution for the car's velocity on a particular track is presented and compared with experimentally measured values.

This analysis has been successfully incorporated into an advanced laboratory project in introductory physics to emphasize the development of model building skills. Details of the project structure, a preliminary assessment of its effectiveness, and suggestions for its implementation are discussed in the conclusions. Although the analysis presented here includes a combination of several effects simultaneously (to briefly document the more sophisticated model), a gradual development of the mathematical model in a case-by-case approach provides a more appropriate learning scenario for students. We note that the models and experimental methods described in this paper are intended for experienced educators who may wish to develop a pedagogical approach that is appropriate for their own students.

At Clarkson, students work in teams of four with occasional guidance from an instructor when their group's progress is slow or halted. Students are encouraged to tackle the project using the same problem solving strategies reinforced in the lecture. Assistance is provided strategically in such a way that allows students initially to develop simple solutions that they will eventually be able to build upon to accommodate additional effects. For example, the simplest development, obtained from only a consideration of the exchange between kinetic and gravitational potential energy, will give way to more sophisticated solutions as more realistic considerations are included (see Table I). As their familiarity with the problem increases, the students gain confidence in their ability to tackle the ''next level,'' are excited about the prospect of doing so, and are open to the notion that they may have to learn new skills to progress. This layered approach allows the instructor the opportunity of tailoring the educational experience according to the interest level and background of the students. Hence, the same project could be presented at a variety of levels ranging from high school physics to an advanced undergraduate experience. The educational value of teaching modeling concepts as a process of progressively increasing the sophistication and accuracy cannot be overemphasized.

II. THEORETICAL MODEL

A typical Matchbox car has a die-cast body, two axles, and four hard plastic wheels, with a total mass of approximately 50 g. Because the combined mass of the wheels is less than 3% of the total mass of the car, we neglect the rotational kinetic energy imparted to them. There are no wheel bearings in a Matchbox car, as the plastic wheels simply rotate on axles that are fixed to the chassis. The weight of the chassis rests on the axles, which in turn slide on the inner holes of the wheels. Consequently, we invoke the traditional sliding friction model, which assumes a kinetic frictional force that is directly proportional to the normal force

$$f_k = \mu_k N, \tag{1}$$

where the constant of proportionality μ_k is the coefficient of kinetic friction.

The flexible plastic track used in this analysis can be rigidly mounted with an appropriate support structure (see Appendix A) in a variety of smooth shapes containing hills and

Table I. Case-by-case model development. The following numerical solutions predict the velocity of the car on an arbitrarily shaped track.

Case	Effects included	Solution
A	Potential energy (PE), kinetic energy (KE)	$v=\sqrt{v_0^2-2g(y-y_0)}$
B	PE, KE, friction	$v=\sqrt{v_0^2-2g(y-y_0)-2g\mu_k(x-x_0)}$
C	PE, KE, friction, track shape	$v=\sqrt{\left[v_0^2\left(1-\frac{\mu_k}{r_0}(x'-x_0')\right)-2g(y-y_0)-2g\mu_k(x-x_0)\right]\Big/\left[1+\frac{\mu_k}{r}(x'-x_0')\right]}$
D	PE, KE, friction, track shape, air resistance	$v=\sqrt{\left[v_0^2\left(1-\left(\frac{\mu_k}{r_0}+\frac{k}{m}\right)(x'-x_0')\right)-2g(y-y_0)-2g\mu_k(x-x_0)\right]\Big/\left[1+\left(\frac{\mu_k}{r}+\frac{k}{m}\right)(x'-x_0')\right]}$

valleys in a vertical plane. The track surface is fairly hard so that work done by the deformation of the wheels and track when in contact is neglected. Relatively shallow sidewalls keep the car from leaving the track. Collision forces between the car and the track sidewall are not modeled separately, but are assumed to contribute in an averaged manner to the combined frictional losses. Tracks are commercially available through a variety of stores or can be fabricated from similarly shaped plastic molding strips.[4]

Conventional fluid dynamics theory describes a power-law dependence of the drag force on velocity:[5,6]

$$D=\tfrac{1}{2}C_d\rho A v^2, \tag{2}$$

where C_d is the drag coefficient, ρ is the fluid density, and A is the cross-sectional area of the object. Equation (2) should be familiar to most students in introductory physics, and its inclusion opens the door for further investigation of the physics behind it. The Reynolds number is the critical factor in determining the nature of this dependence. This dimensionless number is defined as a ratio of inertial to viscous forces given by

$$R=\frac{\rho v l}{\mu}, \tag{3}$$

where l is the characteristic length associated with the cross-section of an object moving with velocity v (relative to the fluid far from the object) in a fluid with dynamic viscosity μ. The drag coefficient depends in a complicated way on the Reynolds number, a topic that is discussed in most textbooks on fluid mechanics.[5,6] For the highly viscous case known as creeping flow ($R\leqslant 1$), inertia forces are negligible, and C_d is inversely proportional to R, resulting in a drag force that is proportional to the velocity. At larger values of R, C_d is approximately constant resulting in a drag force that is proportional to the square of the velocity.

A suitable length scale for a typical car is approximately 3.0 cm, the approximate cross-sectional width. For a car moving through the air at room temperature:[7] $\rho \approx 1.21$ kg/m^3, $\mu \approx 1.81\times 10^{-5}$ kg/m·s. With these values, a car would have to be traveling at a speed of less than 5×10^{-4} m/s to invoke the small Reynolds number limit. We expect the car to spend a negligible amount of time in this regime, perhaps for a brief moment after being released from rest. Consequently, we include a drag force that is proportional to the square of the velocity,

$$D=kv^2, \tag{4}$$

where k is the drag constant and is equal to $(1/2)C_d\rho A$.

To further simplify the analysis, the rotational inertia of the body is neglected. For all intents and purposes, the chassis, wheels, and axles are treated as a single entity, much like a sliding block (a familiar problem for most students) with losses arising from a sliding frictional force and air resistance. The free body diagram is illustrated in Fig. 1 for a car on a small section of a typical track. Some of the assumptions, justified at this stage by qualitative arguments, will ultimately be justified by the agreement of the experimental results with the theory.

The curvature of the track will affect the normal force by inducing a centripetal acceleration of the car. This acceleration in turn will affect the frictional force,

$$f_k=\mu_k m\left(g\cos\theta+\frac{v^2}{r}\right), \tag{5}$$

which increases in the valleys where the curvature is positive and decreases on the hills where the curvature is negative. Here m is the total mass of the car, g is the acceleration due to gravity, θ is the local inclination of the track with respect to the horizontal, and r represents the local radius of curvature.

An application of Newton's second law in the direction parallel to the track, x', yields the equation of motion,

$$mg\sin\theta-f_k-D=ma_{x'}, \tag{6}$$

where the acceleration $a_{x'}$ can be written as

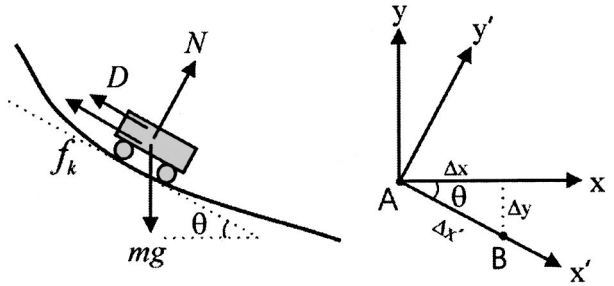

Fig. 1. Free body diagram for a car on a small section of track.

$$a_{x'}=\frac{dv}{dx'}\frac{dx'}{dt}=v\frac{dv}{dx'}=\frac{1}{2}\frac{d(v^2)}{dx'}. \tag{7}$$

Here the time has been eliminated in favor of a spatial description of the acceleration, because we will experimentally measure the velocity of the car at fixed points along the track rather than at different times. The final manipulation of the acceleration term into a spatial derivative of v^2 is merely for our convenience, as we recognize that the velocity dependence of Eqs. (4) and (5) is also quadratic. In our experience, most students are able to understand the importance of eliminating time as a consequence of the nature of the measurements, and proceed accordingly with just the initial manipulation. Learning to express a physical variable in terms of measurable quantities is an important exercise for students to complete. Facilitating this learning process requires careful guidance on the part of the instructor, as students often need assistance with the formalities of proper mathematical expression, even if they understand the underlying concept.

If we combine Eqs. (4)–(7), we obtain the following linear, first-order differential equation:

$$mg\sin\theta-\mu_k mg\cos\theta-\mu_k m\frac{v^2}{r}-kv^2=\frac{m}{2}\frac{d(v^2)}{dx'}. \tag{8}$$

By integrating Eq. (8) with respect to x' (with θ a function of x'), we obtain

$$\frac{m}{2}(v^2-v_0^2)=-mg(y-y_0)-\mu_k mg(x-x_0)-\mu_k m\int_{x_0'}^{x'}\frac{v^2}{r}dx'-k\int_{x_0'}^{x'}v^2dx'. \tag{9}$$

The term on the left and the first term on the right represent changes in the kinetic and gravitational potential energy, respectively. The second term on the right is the work done by kinetic friction and depends only on the horizontal distance traveled by the car. The remaining integrals represent the correction to the work done by kinetic friction on a *curved* surface and work done by the drag force, respectively. The same description could be obtained directly from work–energy considerations. Our experience has been that the latter is the preferred approach for approximately half the student groups. The exercise of formulating the model mathematically generates much discussion among group members about the most appropriate approach, and provides a great opportunity for students to see the connection between Newton's second law and work–energy concepts in the context of a real problem.

At this point, an analytical solution is out of reach for all but the simplest of track shapes. A numerical solution can be obtained given the local radius of curvature for a particular track. An approximate solution valid for small increments in $\Delta x'$ can quickly be achieved by approximating the integrals with simple quadrature. The use of the standard trapezoidal rule leads to a quadratic algebraic equation in v:

$$v=\sqrt{\left[v_0^2\left(1-\left(\frac{\mu_k}{r_0}+\frac{k}{m}\right)(x'-x_0')\right)-2g(y-y_0)-2g\mu_k(x-x_0)\right]\Big/\left[1+\left(\frac{\mu_k}{r}+\frac{k}{m}\right)(x'-x_0')\right]}, \tag{10}$$

where the subscript zero denotes the initial state. The speed of the car at any subsequent point along the track can be evaluated numerically using a simple spreadsheet application if the parameters μ_k and k for a given car and the radius of curvature function r, describing a particular track, are known. If the car is released from rest, Eq. (10) requires the condition $(y_0-y)>\mu_k(x-x_0)$ to be satisfied in order for the car to advance, a familiar condition that essentially defines the static friction coefficient based on the critical angle. In addition, the car will leave the track if the normal force vanishes, invalidating the solution at that point. For any given combination of car and track, this condition should be checked.

Less sophisticated solutions could certainly be achieved (even algebraically if the acceleration is assumed constant over a small displacement) by neglecting the drag force, track shape, or even frictional force in a case-by-case development of the mathematical model. Such a treatment greatly simplifies the derivation of Eq. (9) from Eq. (8), giving students the opportunity to grow into the more sophisticated mathematics, one step at a time. Four cases that emphasize the hierarchical structure of the solutions are summarized in Table I. Most of our students construct their solutions in a similar manner, but they are not required to do so. We intentionally leave the project open-ended to allow their own ideas and creativity to lead their decision-making.

III. DETERMINATION OF PARAMETERS

The parameters k and μ_k for a given car could be obtained independently with the use of a miniature wind tunnel and a vacuum chamber containing a suitable length of track. However, without the use of sophisticated equipment, the parameters can be extracted from velocity measurements using a series of photogates positioned along a straight track. Temporarily restricting our analysis to a *horizontal* straight track eliminates the issue of curvature as well as changes in potential energy. In our experience, some students eventually come to this realization without much assistance, while others need guidance to appreciate the advantage of this simplification. In any event, actually designing an experimental procedure that takes advantage of this concept does not come naturally, as most students at this level lack experience designing their own experiments. Rather than providing them with a ''recipe,'' we guide them with an inquiry-based approach, leading them toward the development of a successful experiment, often allowing them to make critical mistakes along the way. This process is time consuming as each group chooses a different path, but the experience helps them to realize the importance of a well-designed experiment and

Table II. Case-by-case development for experimental method.

Case	Simplified solution for a horizontal straight track	Needed parameters	Method
A	$v^2=v_0^2$	None	None
B	$v^2=v_0^2-2\mu_k g(x-x_0)$	μ_k	Linear least-squares fit to experimentally obtained plot of v^2 vs x data
C	$v^2=v_0^2-2\mu_k g(x-x_0)$	μ_k	Linear least-squares fit to experimentally obtained plot of v^2 vs x data
D	$v^2=\left(v_0^2+\frac{\mu_k mg}{k}\right)e^{-(2k/m)(x-x_0)}-\frac{\mu_k mg}{k}$	μ_k, k	Nonlinear least-squares fit to experimentally obtained plot of v^2 vs x data

ultimately gives them a sense of ownership over the project. Below we document one method for determining the necessary parameters for the more sophisticated model, although in practice we encourage students to pursue a case-by-case approach that works hand-in-hand with their theoretical development (see Table II). Most of our students construct their experimental protocol in a similar, but not necessarily identical manner.

Consider the experimental setup depicted in Fig. 2, where a car is released at some initial height, but the analysis is restricted to the flat portion of the track. With this simplification, Eq. (8) can be solved exactly for v^2:

$$v^2=\left(v_0^2+\frac{\mu_k mg}{k}\right)e^{-(2k/m)(x-x_0)}-\frac{\mu_k mg}{k}. \tag{11}$$

Extracting the relevant values for the friction coefficient and drag constant does not appear to be straightforward from Eq. (11) due to the way in which the parameters appear. However, note that the solution has the form

$$v^2(x)=(A+B)e^{-Cx}-B, \tag{12}$$

when x_0 is taken to be zero. The constants A, B, and C are

$$A=v_0^2, \tag{13}$$

$$B=\frac{\mu_k mg}{k}, \tag{14}$$

$$C=\frac{2k}{m}. \tag{15}$$

If we assume that the data follows the nonlinear relation described by Eq. (12), a least-squares fit of this form to the experimental measurements would identify the most appropriate values for A, B, and C, from which the needed parameters μ_k and k can be extracted. The details of the least-squares analysis are included in Appendix B.

The experimental setup depicted in Fig. 2 consists of a long track with an initial steep downhill ramp flattening into a straight horizontal section for 5 m. A 1 cm wide plastic flag, rigidly mounted to the top of the car (see Fig. 3), trips the photogates spaced at 10 cm intervals along the flat section of the track. In our setup, the photogates are connected to a computerized data acquisition system. However, any system of photogates set to measure the amount of time the flag spends in each gate is suitable. The measured speed is approximated as the ratio of the effective flag width to the measured time. A more detailed description of the experimental setup is provided in Appendix A.

To measure a range of speeds up to approximately 5 m/s (the maximum expected speed for our particular setup), it was necessary to collect several data sets by releasing the car from different starting heights as depicted in Fig. 2. In order to cover the full range of speeds for a typical car in a *single* run (beginning with an initial speed of 5 m/s and allowing the car to come almost to rest), we would have needed a flat section of track approximately 22 m long. To circumvent this limitation, we simply chose a series of starting heights that ensured suitable overlap in the measurements by making certain that the new initial speed was slightly higher than the final speed obtained from releasing the car at the previous height. This approach required that the car be released from a total of five different starting heights. To ensure that we

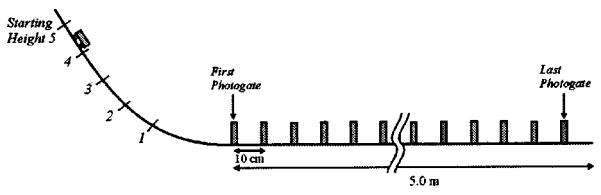

Fig. 2. Experimental setup used to determine the parameters μ_k and k for a given car.

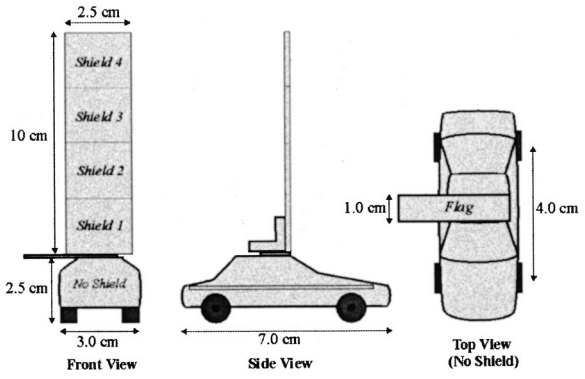

Fig. 3. Schematic views of a typical car with added shields to accentuate the affects of air resistance.

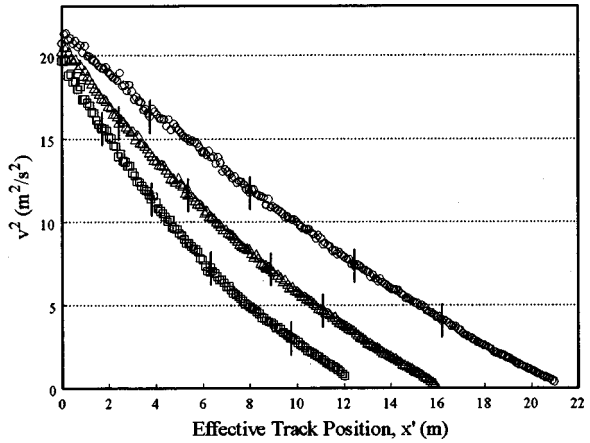

Fig. 4. Velocity squared versus effective track position for the *No-Shield* (○), *Shield-2* (△), and *Shield-4* (□) configurations. The vertical lines indicate where data sets have been appended.

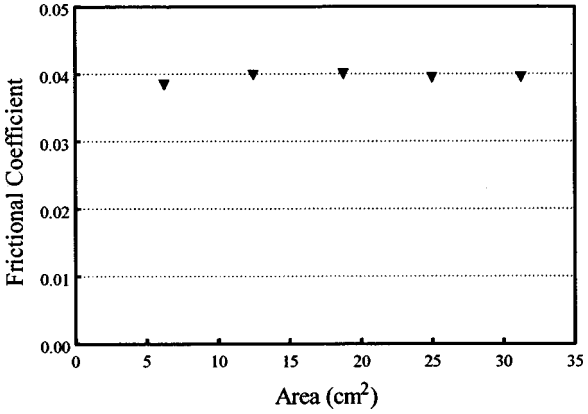

Fig. 5. Experimentally determined friction coefficient μ_k versus cross-sectional area A. Each data point represents a different car-shield configuration.

had decent statistical data, we ran 20 trials from each starting height. Less ambitious groups who fail to collect data over a wide enough range of speeds will end up with a larger margin of error in their determination of the important parameters and ultimately in their model predictions. For many teams, this realization occurs after they have already collected their data. The more careful teams end up repeating the experiment with a newly improved and more appropriately designed experimental procedure.

To accentuate the effects of air resistance, rigid rectangular plastic shields with increasing cross-sectional area were mounted to the top of the car and the experiment was repeated (see Fig. 3). The cross-sectional area of the car measured approximately 6.25 cm^2, and each individual shield increased this area by approximately the same amount. Complete data sets covering the full range of speeds were collected for five different cross-sectional areas. The results are presented in Fig. 4. The vertical lines mark the places where individual data sets have been appended. Even in the absence of a shield, the data deviates from the linear relation that is predicted when the effects of air resistance are neglected in the mathematical model (see below). This deviation, observed over a broad range of velocities, captures the influence of the drag force on the car's performance. Only three of the five complete sets obtained for the different cross-sectional areas have been included to avoid unnecessary clutter in the figure, although the extracted values of μ_k and k have been tabulated for all the sets in Table III.

We expect the measured kinetic friction coefficient to be constant, because it should be independent of the shield configuration. For the car we tested, μ_k varies by less than 3% from its average value as shown in Fig. 5, while the drag constant is proportional to the cross-sectional area as shown in Fig. 6. The consistency of the extracted parameters with the expected trends is both reassuring and exciting, adding credence to the chosen model.

Note that if we neglect the effect of air resistance on the car's performance by setting k equal to zero in Eq. (8), the integration gives the much simpler solution:

$$v^2 = v_0^2 - 2\mu_k g(x - x_0), \tag{16}$$

which contains the single parameter μ_k. Equation (16) predicts a linear relationship between v^2 and x, with the slope equal to $-2\mu_k g$. Hence, μ_k can be quickly extracted from a simple linear fit to the v^2 vs x data and implemented in the Case B and C models presented in Table I which neglect the drag force. A case-by-case development of the experimental method is summarized in Table II.

Table III. Parameters for different car-shield configurations. In this table, m represents the total mass of the car-shield configuration.

Configuration	Area (cm^2)	m (kg)	μ_k	k (kg/m)
No-shield	6.25	0.0495	0.0384	0.00065
Shield-1	12.50	0.0548	0.0399	0.00109
Shield-2	18.75	0.0556	0.0399	0.00154
Shield-3	25.00	0.0564	0.0394	0.00214
Shield-4	31.25	0.0573	0.0395	0.00272

IV. NUMERICAL SOLUTION FOR A PARTICULAR TRACK

To test the predictive capability of the general model in Eq. (10) with the newly measured parameters, we chose a 4.0 m long track having two valleys separated by a single hill (see Fig. 7). The track shape was digitized against a back-

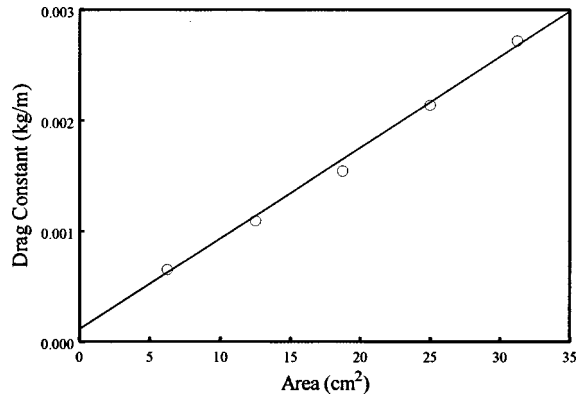

Fig. 6. Experimentally determined drag constant k versus cross-sectional area A. Each data point represents a different car-shield configuration. The solid line is a linear least-squares fit.

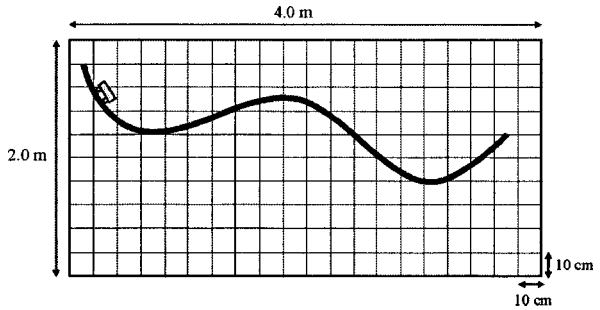

Fig. 7. An arbitrary track shape.

ground grid (see Appendix A) and fit with a least-squares polynomial approximation to determine the curvature function κ, defined as

$$\kappa = \frac{1}{r} = \frac{d^2y/dx^2}{\{1+[dy/dx]^2\}^{3/2}}. \tag{17}$$

The numerical solution shows good agreement with measured values of velocity, as shown in Fig. 8 for the no-shield and shield-4 configurations. The error bars of the measured data do not exceed the size of the symbols in the graph. All calculations were carried out for small increments in Δx of 1×10^{-4} m. Most students pursuing the model at this level will need to spend some time researching the topic of curvature. At Clarkson, students are encouraged to seek out such information from a variety of resources ranging from calculus texts to math professors. The implementation of this information as well as the least-squares analysis is typically completed with software packages such as Microsoft® Excel or MATLAB® depending on individual team preference. Again, a recipe is not provided, but groups are encouraged to learn the necessary tools to complete the project.

Table IV documents the average and maximum percent difference between each numerical prediction, and the measured values of the velocity for all car-shield configurations. The differences between the predicted and measured values can be attributed to the neglect of rotational kinetic energy imparted to the wheels and general rotation of the car body. The correlation between the increase in error with the cross-sectional area of the respective shields is likely to arise from the propensity for the car to tip at certain speeds, resulting in a distribution of forces different than the assumed model.

Table IV. Percent difference between predicted and measured velocities.

Configuration	Avg. percent diff.	Max. percent diff.
No-shield	1.2	3.0
Shield-1	1.2	3.0
Shield-2	1.0	4.5
Shield-3	2.4	6.1
Shield-4	2.4	7.1

If we assume the resultant drag force acts through the centroid of the cross-sectional area of the car-shield configuration, a torque of increasing magnitude will be produced as the shield size is increased. Because the car actually makes contact with the track through the set of two wheels in front and two wheels in back, this torque could have the effect of tipping the car backward if the drag force reaches some critical value. This value translates to a critical speed that can be estimated for the car on a horizontal track as

$$v_{\text{critical}} = \sqrt{\frac{mgl}{2kh}}, \tag{18}$$

where l is the center-to-center distance between the axles and h is the height of the centroid. If the car reaches this critical speed, it will presumably tilt. See Appendix C for details of this calculation. For our car in the shield-4 configuration ($h = 6.25$ cm, $l = 4.25$ cm), the estimated critical speed is approximately 9.0 m/s, more than double the maximum speed experienced. However, even for speeds below the critical value, the redistribution of forces could be important for the large shield configurations.

The evolution of the work done by each nonconservative term in Eq. (9) is shown in Fig. 9, and reveals the relative importance of each effect included in the model. In the absence of a shield, the work done by the drag force is minimal as expected, accounting for less than 16% of the net loss in mechanical energy by the time the car reaches the end of the track. The correction to the work done by friction varies according to the curvature of the track, accounting for 33% of this net loss in the end. The bulk of the loss (51%) is attributed to the frictional term that depends only on the

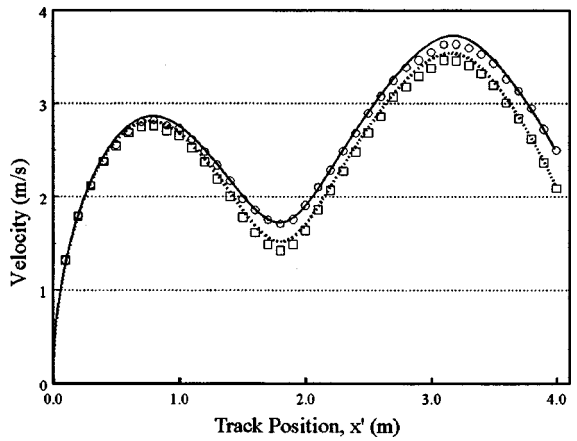

Fig. 8. Numerical solution for the car traveling on the arbitrary track shape in comparison to the measured values of velocity for *No-Shield* (○) and *Shield-4* (□) configurations.

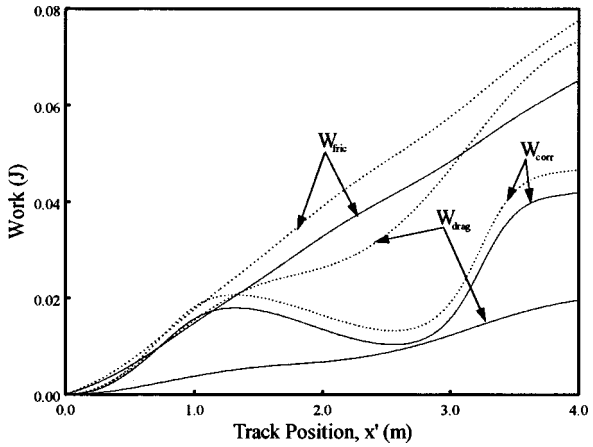

Fig. 9. The work done by kinetic friction, the correction to the work done by kinetic friction due to the curvature of the track, and the work done by the drag force for the *No-Shield* (solid) and *Shield-4* (dotted) configurations.

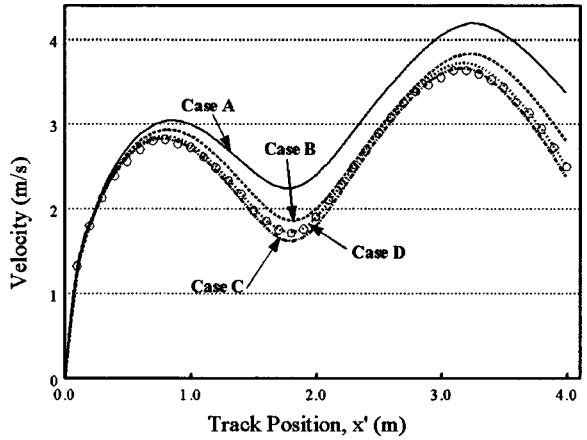

Fig. 10. Numerical solutions for the car traveling on the arbitrary track shape for the cases listed in Table I, compared with the measured values of the velocity for the *No-Shield* (○) configuration.

horizontal distance traveled by the car. In contrast, the work done by the drag force for the shield-4 configuration clearly dominates the 24% loss from the correction term, now accounting for approximately 37% of the net loss in the end, nearly matching the 39% imparted to the remaining frictional term. This type of analysis is important in helping students to understand the nature of model development, and emphasizes the importance of capturing the most dominant effects first.

In Fig. 10 we present the numerical solutions for the four cases given in Table I, and compare them with the experimental measurements. To avoid redundancy, we have only included results for the no-shield configuration. However, the excellent agreement achieved with Case D was equally common to the other configurations. As expected, each case produces a slight correction to the previous one, with Case D giving the most accuracy. In fact, Case C does quite well in mimicking the velocity of the car in the absence of a mounted shield. Viewing the contributions of each case in a comparison study reinforces the modeling process for students, who are often excited to see the improvements of their latest model.

The predicted normal force shown in Fig. 11 demonstrates the effect of track curvature on the frictional force experienced by the car. In particular, we have plotted the normal force for the no-shield configuration as a function of position

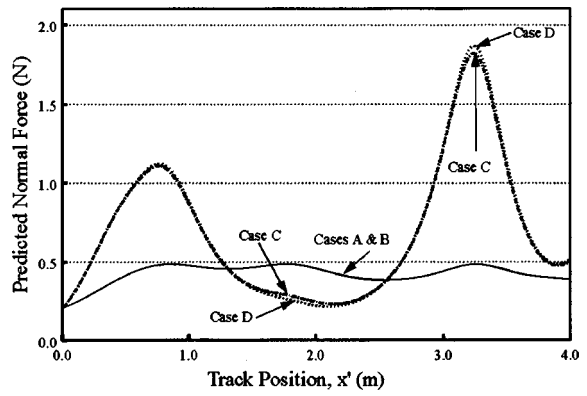

Fig. 11. Predicted normal force for the car traveling on the arbitrary track shape for the cases listed in Table I (*No-Shield* configuration).

on the track for the various cases. The failure of Case B to include the curvature of the track leads to a gross underestimation of the normal force and thus the work done by friction in certain regions of the track, accounting for this model's poorer agreement with the measured velocity data (see Fig. 10). Note that the predicted normal force never vanishes, assuring that this car remains on this track throughout the segment considered, and indeed it did. The maximum predicted normal force of 1.9 N for the no-shield configuration suggests that occupants of this vehicle would encounter a 2.8 g acceleration, characteristic of a roller-coaster type experience.

V. CONCLUSIONS

Without the use of sophisticated equipment, a given toy car's effective friction coefficient and drag constant can be ascertained from velocity measurements made with a series of photogates. A least-squares extraction of the necessary parameters from the consideration of the motion on a horizontal straight track provides a reasonable prediction of the car's performance on an arbitrarily shaped track for motion restricted to a vertical plane. Inclusion of the kinetic energy imparted to the rotation of the wheels is fairly straightforward if the rotational inertia is known or estimated, but is not necessary to achieve satisfactory results, because the additional contribution is on the order of the measured error.

The modeling concepts and experimental investigations presented here have been successfully incorporated into an advanced group project for an introductory course in classical mechanics at Clarkson University. This project stems from a departmental initiative to develop an educational program centered on project-based learning from which students can learn and develop basic modeling skills. The pedagogical approach is inquiry-based and emphasizes experiential learning, open-ended problem solving, and the development of analytical and collaborative learning skills, providing students with an educationally richer and more challenging experience than is typically obtained in the traditional laboratory environment.

Students who choose to take part in the project work in groups of four as members of an investigating team for a period of 10 weeks. The project serves as the major portion of their laboratory requirement, although other laboratory exercises/projects are included that reinforce the modeling approach. Out of a course of approximately 500 students, 60 students participated in the project. The *Force Concepts Inventory*[8] (FCI) was used as a diagnostic tool to assess the performance of students who completed the project compared with a statistically comparable group of students who did not. The comparison group was formed from students who had SAT and pre-test FCI scores comparable to those of the participating students. Preliminary assessment data suggests that students who participated in the project out performed the comparison group by a factor of 1.5 and the rest of the class by a factor of 1.6, based on the traditional percent gain calculation. In particular, examination of the individual gains for the six conceptual dimensions identified by Hestenes *et al.*[8] reveals that the participating students outperformed the rest of the class by a factor of 1.9 in the categories of *Kinematics* and *Newton's Second Law*, the two areas most emphasized by the project. We expect to publish a more

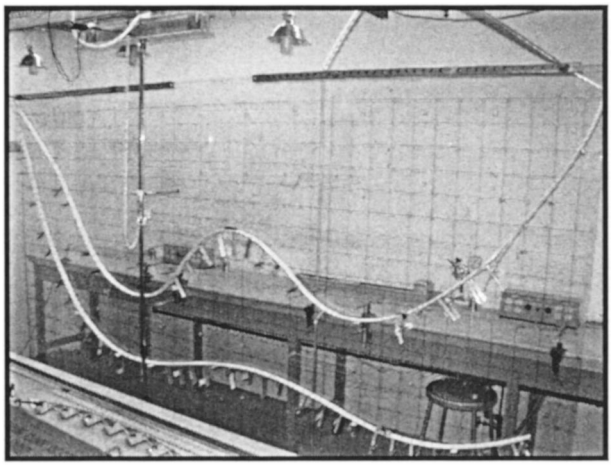

Fig. 12. Picture of experimental setup with mounted tracks.

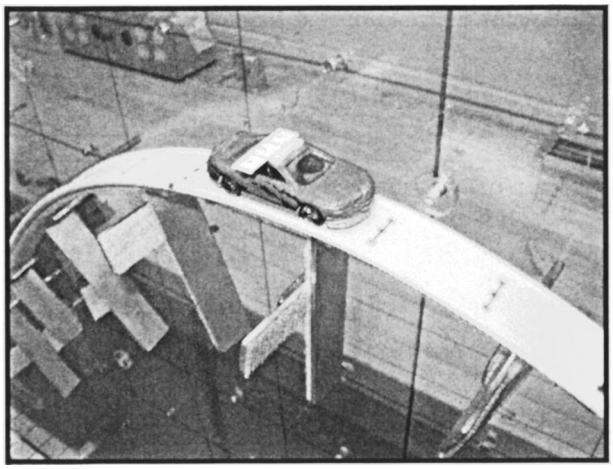

Fig. 13. Close-up picture of the track support structure.

comprehensive evaluation of the pedagogical approach as well as additional suggestions for successful implementation of the project in a future article.

Perhaps the most important benefit of this particular project is that it lends itself nicely to a multi-layered development. Although the full analysis, which includes many effects simultaneously (as presented here), may appear challenging for an introductory physics course, a gradual development can be effectively achieved in the classroom/laboratory environment. The development of the model in a case-by-case approach that incrementally includes different effects emphasizes a hierarchical structure to the solutions. Simpler solutions (such as that obtained from considering only the exchange between kinetic and gravitational potential energy) will give way to more sophisticated solutions (such as those obtained from the consideration of friction, track shape, and air resistance) that can be pursued according to the general interest level and background of the students. In addition, students that pursue the more advanced models are introduced to a variety of mathematical techniques such as least-squares analysis and integral approximations. A careful analysis provides an assortment of additional interesting topics to be pursued, including the prediction of cars that will leave the track and the determination of a critical speed when the car will begin to tilt.

Each toy car has unique characteristics and will consequently perform differently from other cars on any given track shape. This difference has the advantage of allowing the instructor to develop a series of challenges for the students, where the solutions will be unique for each group. At Clarkson, the challenges are administered in a competitive environment to see which teams are most successful at predicting the performance of their car on track shapes that they have not seen before. For example, students are asked to predict turning points for their cars traveling on tracks ranging from the simplest of shapes where the curvature is constant (semicircular tracks) to more complicated shapes containing multiple hills and valleys. The latter case is particularly interesting if the track is carefully designed with a large central hill surrounded by two valleys such that only some of the cars will make it over the hill. As an example, see the upper track displayed in Fig. 12. Having students place a one-dimensional bulls-eye next to the predicted location provides a mechanism for awarding points to the most successful groups. In this phase of the project, teams are given an electronic copy of the digitized track shapes one week in advance of the challenge sessions in preparation for the competition. The success of each group depends largely on the extent to which they have developed their model, their understanding of the predictive capability of their model, and the care that they have taken in determining the experimental parameters. Of course, results also depend on the care that is taken of the car during the testing phase. A dropped car could have a significantly different friction coefficient than it had originally due to a slightly bent axle or misaligned wheel. Properly placed safety nets minimize damage to cars that fly off the track. Other challenges require teams to predict release points on a given track shape to accomplish jumps over obstacles or through target windows, soft cushioned barrel jumps, or even timing events. An event designed with a U-shaped track could require groups to predict the number of times their car will oscillate back and forth along the track before coming to rest. More challenging events include loop-the-loop sections of track. Each semester, students look forward to competing in the challenge sessions, which provide a sort of grand finale to the semester-long project.

ACKNOWLEDGMENTS

This project continues to be funded by the School of Science at Clarkson University, through the generous support of Provost, A. Collins. The authors are indebted to J. Hruska for his time, dedication, and expertise. His attention to detail and contributions to the development of quality equipment have played a crucial role in the success of this endeavor. We are further grateful to L. S. Schulman, D. ben-Avraham, T. Lakoba, D. Cole, and especially our students for their suggestions and encouragement.

APPENDIX A: DETAILS OF THE EXPERIMENTAL SETUP

The experimental setup consists of a vertical Plexiglas wall assembled from three commercially available 4.0 ft $\times$8.0 ft sheets as shown in Fig. 12. A 3.5 m$\times$2.0 m region of this wall is superimposed with a 10 cm$\times$10 cm grid. A series of 3/8 in. peg holes are spaced according to the layout of the grid. A system of rigid pegs and right angle supports covered

with Velcro™ are used to provide support for the flexible track, the underside of which is also covered with Velcro (see Fig. 13).

It is important to note that the distance the car moves as measured by the signaling photogate is *not* exactly equivalent to the physical width of the flag. The infrared beam of light emitted by the photogate sensor has its own width, which switches the gate OFF when some critical percentage of the light is blocked. Essentially, each sensor ''sees'' an effective flag width that is slightly less than the actual flag width. This effective flag width can be measured with a micrometer-scale measuring device by noting the car's position when the signal first vanishes and then reappears for each gate. The process is time consuming, but important. After averaging several measurements for a variety of gates, we obtained an effective flag width of 0.88 cm, a significantly smaller distance than the physical width of 1.0 cm. Due to the high velocities of the car and the small flag size, we sampled at a frequency of 400 kHz to give us approximately 800 readings per gate occupancy, providing an uncertainty of ± 0.006 m/s at the 5 m/s speed. The accuracy increases as the velocity decreases due to the increased number of readings per occupancy.

APPENDIX B: LEAST-SQUARES ANALYSIS

We wish to find the values of A, B, and C that will minimize the sum of squares,

$$S=\sum_{i=1}^{N}\,(v_i^2-v^2(x_i))^2=\sum_{i=1}^{N}\,(v_i^2-[(A+B)e^{-Cx_i}-B])^2, \tag{B1}$$

where v_i^2 represents the measured data and $v^2(x_i)$ represents the predicted values at the location of the corresponding N measured values. At the minimum of this three-dimensional parameter space, the following partial derivatives must vanish:

$$\frac{\partial S}{\partial A}=0=\sum_{i=1}^{N}\,2\{v_i^2-[(A+B)e^{-Cx_i}-B]\}e^{-Cx_i}, \tag{B2}$$

$$\frac{\partial S}{\partial B}=0=\sum_{i=1}^{N}\,2\{v_i^2-[(A+B)e^{-Cx_i}-B]\}(1-e^{-Cx_i}), \tag{B3}$$

$$\frac{\partial S}{\partial C}=0=\sum_{i=1}^{N}\,2\{v_i^2-[(A+B)e^{-Cx_i}-B]\}(A+B)\times(x_i)e^{-Cx_i}. \tag{B4}$$

The term $(A+B)$ can be isolated in Eq. (B2) to have the form

$$(A+B)=\frac{\Sigma_{i=1}^{N}(v_i^2+B)e^{-Cx_i}}{\Sigma_{i=1}^{N}e^{-2Cx_i}}. \tag{B5}$$

If we add Eqs. (B2) and (B3), we obtain the much simpler form:

$$\sum_{i=1}^{N}\,\{v_i^2-[(A+B)e^{-Cx_i}-B]\}=0, \tag{B6}$$

which can be combined with Eq. (B5) to obtain an expression for B in terms of C:

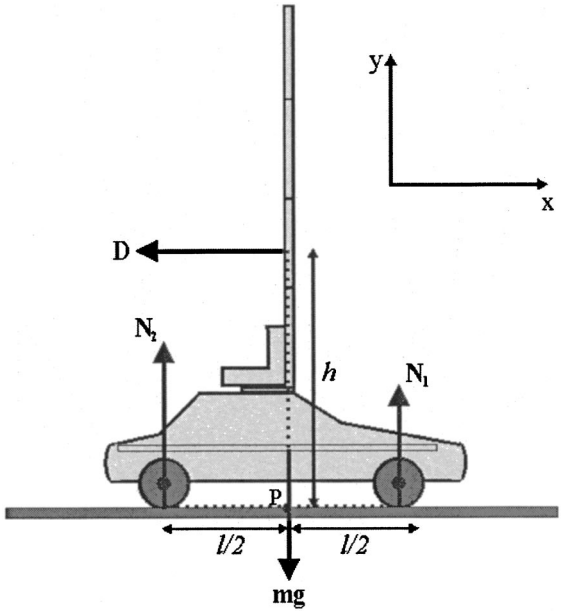

Fig. 14. Free body diagram for a car on a horizontal track assuming two separate normal forces and a drag force acting through the centroid of the cross-sectional area.

$$B=\frac{\Sigma_{i=1}^{N}v_i^2\Sigma_{i=1}^{N}e^{-2Cx_i}-\Sigma_{i=1}^{N}v_i^2e^{-Cx_i}\Sigma_{i=1}^{N}e^{-Cx_i}}{(\Sigma_{i=1}^{N}e^{-Cx_i})^2-N\Sigma_{i=1}^{N}e^{-2Cx_i}}. \tag{B7}$$

We then substitute Eq. (B7) and Eq. (B5) into Eq. (B4) to produce an equation containing the single parameter C. Although the resulting equation cannot be solved directly for C, a parameter search can be conducted numerically to find the appropriate value that will make the resulting function vanish. Once C is found, B and A can be obtained quickly from Eqs. (B7) and (B5), allowing the parameters μ_k and k for a particular car to be determined.

APPENDIX C: CRITICAL VELOCITY CALCULATION

To estimate the critical speed at which the car-shield configuration will begin to tip on a horizontal track, it is necessary to employ a slight correction to the model by incorporating *two* normal forces. The car makes contact with the track through a set of front and rear wheels. These contacts can be characterized by two normal forces denoted as N_1 and N_2 as shown in Fig. 14, where l is the center-to-center distance between the axles. If we still neglect the rotational kinetic energy imparted to the wheels, we can treat the two sets of wheels as fixed, rigid attachments, upon which the whole system slides. The resultant drag force acts through the centroid of the cross-sectional area of the car-shield configuration, producing a torque that could tip the car backward. Such an effect will occur if N_1 vanishes. The centroid height is denoted as h in Fig. 14. We assume the mass is evenly distributed across both sets of wheels. If we apply Newton's second law in the y direction, we obtain

$$N_1+N_2-mg=0. \tag{C1}$$

Similarly, we sum the torques about point P and find

$$kv^2h+N_1\frac{l}{2}-N_2\frac{l}{2}=0. \tag{C2}$$

If we eliminate N_2, we obtain the following relation for N_1:

$$N_1=\frac{mg}{2}-kv^2\frac{k}{l}. \tag{C3}$$

By considering the condition for which N_1 vanishes, the estimated critical speed is obtained:

$$v_{\text{critical}}=\sqrt{\frac{mgl}{2kh}}. \tag{C4}$$

[a)]Electronic mail: wickdp@clarkson.edu

[1]P. Theodórsson, "A new dynamics cart on an inclined plane," Phys. Teach. **33**, 458–459 (1995).
[2]R. F. Larson, "Measuring the coefficient of friction of a low-friction cart," Phys. Teach. **36**, 464–465 (1998).
[3]B. S. Andereck, "Measurement of air resistance on an air track," Am. J. Phys. **67**, 528–533 (1999).
[4]For example, track sets from Matchbox, Hot Wheels, and Darda are commercially available at a variety of toy and discount stores.
[5]F. M. White, *Fluid Mechanics*, 2nd ed. (McGraw-Hill, New York, 1986), pp. 264–268, pp. 411–431.
[6]R. W. Fox and A. T. McDonald, *Introduction to Fluid Mechanics*, 5th ed. (Wiley, New York, 1998), pp. 444–452.
[7]R. W. Fox and A. T. McDonald, *Introduction to Fluid Mechanics*, 5th ed. (Wiley, New York, 1998), p. 707.
[8]D. Hestenes *et al.*, "Force concepts inventory," Phys. Teach. **30**, 141–157 (1992).

HISTORY, UNIVERSALITY, AND THE UNIVERSE

If we restrict ourselves to proposals which are falsifiable, what kind of explanations are available to us? In the history of science there have been two kinds of explanations which generally succeeded: explanations in terms of general principles; and explanations in terms of history. We are used to believing that the former are more fundamental than the latter. If we discover a fact that seems to hold universally, such as that all electrons have the same mass, we believe immediately that the reason for it must rest on principle and not on history. We usually expect a phenomenon to be contingent only if we see that it changes from instance to instance. If asked to justify this, we would say that something that is universally true cannot rest on contingent circumstances, which can vary from case to case. This makes sense, but it is an example of the kind of argument that works well only as long as it is not applied at the scale of the universe as a whole. When we are dealing with properties of the observable universe we no longer have any reason to insist that if something is true in every observable case, it cannot at the same time be contingent. One reason is that we have no justification to assert that the universe we see around us represents a good sample of all that exists, or that has existed, or that might in principle exist. There is in fact no logical reason to exclude the possibility that some of the facts about the elementary particles, which appear to hold throughout our observable universe, might at the same time be contingent.

Lee Smolin, *The Life of the Cosmos* (Oxford University Press, New York, NY, 1997), p. 77.